A&A 642, L8 (2020)
https://doi.org/10.1051/0004-6361/202039274

Astronomy & Astrophysics

LETTER TO THE EDITOR

Discovery of HC_4NC in TMC-1: A study of the isomers of HC_3N, HC_5N, and HC_7N★

J. Cernicharo[1], N. Marcelino[1], M. Agúndez[1], C. Bermúdez[1], C. Cabezas[1], B. Tercero[2,3], and J. R. Pardo[1]

[1] Grupo de Astrofísica Molecular, Instituto de Física Fundamental (IFF-CSIC), C/ Serrano 121, 28006 Madrid, Spain
e-mail: jose.cernicharo@csic.es
[2] Centro de Desarrollos Tecnológicos, Observatorio de Yebes (IGN), 19141 Yebes, Guadalajara, Spain
[3] Observatorio Astronómico Nacional (OAN, IGN), Madrid, Spain

Received 27 August 2020 / Accepted 11 September 2020

ABSTRACT

We present a study of the isocyano isomers of the cyanopolyynes HC_3N, HC_5N, and HC_7N in TMC-1 and IRC+10216 carried out with the Yebes 40m radio telescope. This study has enabled us to report the detection, for the first time in space, of HCCCCNC in TMC-1 and to give upper limits for HC_6NC in the same source. In addition, the deuterated isotopologues of HCCNC and HNCCC were detected, along with all ^{13}C substitutions of HCCNC, also for the first time in space. The abundance ratios of HC_3N and HC_5N, with their isomers, are very different in TMC-1 and IRC+10216, namely, $N(HC_5N)/N(HC_4NC)$ is ~300 and ≥2100, respectively. We discuss the chemistry of the metastable isomers of cyanopolyynes in terms of the most likely formation pathways and by comparing observational abundance ratios between different sources.

Key words. molecular data – line: identification – ISM: molecules – ISM: individual objects: TMC-1 – stars: individual: IRC+10216

1. Introduction

Millimeter-wave observations of lines from isomers of abundant molecular species provide key information for studying the chemical paths leading to their formation in interstellar and circumstellar clouds, an important piece of the astrochemical puzzle. The best known example is that of HCN and HNC, which are formed in interstellar clouds by the dissociative recombination of a common species, the $HCNH^+$ cation, in a branching ratio of 1:1. Once these species are formed, they undergo various reactions that can lead to changes in the initial abundances, in particular, reactions of HNC with atoms and radicals (see, e.g. Hacar et al. 2020 and references therein). In circumstellar clouds, HCN and HNC are produced very close to the photosphere of the central star under thermodynamical chemical equilibrium with a branching ratio of ~1000:1 (Cernicharo et al. 2013). While HCN maintains its abundance across the envelope, HNC disappears very quickly when moving away from the star. It reappears again in the zone where galactic UV photons are able to penetrate the envelope, initiating a very rich photochemistry (Cernicharo et al. 2013).

Some isomers may not necessarily be formed from a common precursor but as an effect of radiation as it is thought to occur for the *cis* conformer of HCOOH in the Orion Bar photodissociation region (Cuadrado et al. 2016). This is an interesting case, in which the absorption of a UV photon by the *trans* conformer leads, through radiative decay, to the *cis* conformer. This photochemical switch can only work in regions with enough UV illumination. In fact, *cis* HCOOH has been detected in the cold dark clouds B5 and L483 (Taquet et al. 2017; Agúndez et al. 2019). The lack of UV photons in these environments together with their derived lower *cis*-to-*trans* abundance ratios, as compared to the Orion Bar, indicate that a different mechanism must operate in these cold clouds.

However, most of the isomers known in space involve radical CN. In addition to HCN and HNC, the isocyanide isomers of CH_3CN (Cernicharo et al. 1988), HC_3N (Kawaguchi et al. 1992a,b), and NCCN (Agúndez et al. 2018) have been detected in space. HCCNC and HNCCC, the two isomers of HC_3N, have also been detected towards the circumstellar envelope IRC+10216 (Gensheimer 1997a,b). A comparative study of the abundances of isomers in interstellar and circumstellar clouds provide an opportunity to understand the chemical processes leading to their formation, as the chemistry prevailing in cold interstellar clouds (ion-neutral reactions) and in external layers of circumstellar envelopes (radical-neutral and photochemical reactions) are very different. In this Letter, we present a systematic study of the HC_3N, HC_5N, and HC_7N isomers, along with their isotopologues, towards TMC-1 and IRC+10216 making use of the observations described in Sect. 2. In Sect. 3 we report on the first detection in space of HC_4NC[1], Isocyanodiacetylene, which is the most stable isomer after HC_5N. This new molecular species has been detected only towards TMC-1, whereas a very low upper limit has been obtained towards IRC+10216, which is a rather interesting finding and which we discuss in Sect. 4.

★ Based on observations carried out with the Yebes 40m telescope (projects 19A003, 19A010, 20A014). The 40m radiotelescope at Yebes Observatory is operated by the Spanish Geographic Institute (IGN, Ministerio de Transportes, Movilidad y Agenda Urbana).

[1] After the original submission of this manuscript and prior to its review, we learned about a parallel effort by Xue (2020) using the GBT at lower frequencies. Their stacked data of three lines present a convincent detection of HC_4NC in TMC-1. The column density they derive is consistent with that from our more complete study of the isomers, isotopologues, and chemistry of cyanopolyynes in this source and toward IRC+10216.

2. Observations

New receivers, built within the Nanocosmos project[2] and installed at the Yebes 40m radio telescope (hereafter, Yebes 40m) were used for the observations of TMC-1. The *Q*-band receiver consists of two HEMT cold amplifiers covering the 31.0–50.3 GHz band with horizontal and vertical polarizations. Receiver temperatures vary from 22 K at 32 GHz to 42 K at 50 GHz. The spectrometers are 2×8×2.5 GHz FFTs with a spectral resolution of 38.1 kHz providing the whole coverage of the *Q*-band in both polarizations. The main beam efficiency varies from 0.6 at 32 GHz to 0.43 at 50 GHz. The beam size of the telescope is 56″ and 36″ at 31 and 50 GHz, respectively. Pointing errors are always within 2–3″.

The observations leading to the *Q*-band line survey towards TMC-1 were performed in several sessions, between November 2019 and February 2020. The observing procedure was frequency switching with a frequency throw of 10 MHz. The nominal spectral resolution of 38.1 kHz was left unchanged for the final spectra. The sensitivity, σ, along the *Q*-band varies between ~0.6 (31 GHz), ~1.0 (43 GHz), and ~2.5 mK (50 GHz). It was derived by removing a polynomial baseline in velocity windows of −6.2 to 17.8 km s^{-1} centered on each observed line.

The intensity scale, antenna temperature (T_A^*), was calibrated using two absorbers at different temperatures and the atmospheric transmission model (ATM, Cernicharo 1985; Pardo et al. 2001). Calibration uncertainties are estimated to be within 10%. All data were analyzed using the GILDAS package[3]. The observations in the *Q*-band of IRC+10216 were previously described by Cernicharo et al. (2019) and Pardo et al. (2020).

3. Results

The sensitivity of our observations towards TMC-1 (see Sect. 2) is a factor of 5–10 better than previously published line surveys of this source at the same frequencies (Kaifu et al. 2004). This has allowed us to detect a forest of weak lines, most of them arising from the isotopologues of abundant species such as HC_3N and HC_5N. For the observed line parameters of HC_3N and its isotopologues, see Appendix B. With regard to HC_5N, in addition to its deuterated species, it has five ^{13}C and one ^{15}N isotopologues and is responsible for 50 features detected within our survey with a signal to noise ratio (S/N) between 10 for $HC_5^{15}N$, 20–40 for the ^{13}C isotopologues, and >1000 for the main isotopologue (see also Appendix B for their observed line parameters). From the seven rotational transitions of HC_5N observed within the *Q*-band (J_{up} = 12 to J_{up} = 18), we obtained a local standard of rest velocity of the source, namely, v_{LSR}, of 5.83 ± 0.01 km s^{-1}. From the ^{13}C and ^{15}N isotopologes of HC_5N, which provide 43 different transitions to estimate this same velocity, we get v_{LSR} = 5.84 ± 0.01 km s^{-1}. Hence, we adopt a value v_{LSR} of 5.83 km s^{-1} for further frequency determinations in TMC-1 (see also Cernicharo et al. 2020). The value given by Kaifu et al. (2004) is 5.85 km s^{-1}, which is practically identical to our result within the observational uncertainties.

3.1. The isomers of HC_3N

The most stable isomers of HC_3N are HCCNC and HNCCC. They have been extensively observed in the laboratory. Rotational transitions of HCCNC have been measured up to J_{up} = 33 at a frequency of 327.8 GHz (Guarnieri et al. 1992). HNCCC is a quasi-linear species, with the hydrogen atom slightly bent with respect to the NCCC axis. Its rotational transitions have been measured in the microwave domain (Hirahara et al. 1993) and at millimeter wavelengths (Vastel et al. 2018). Hence, accurate frequencies are available for these species. The J = 1–0 line of nine HCCNC isotopologue (D, ^{13}C and ^{15}N) was measured in the laboratory by Krüger et al. (1992). The millimeterwave spectrum of DCCNC was measured by Huckauf et al. (1998) up to J_{up} = 51. The microwave spectrum of DNCCC was measured by Hirahara et al. (1993) up to J_{up} = 2, and ν_{max} = 19 GHz. The derived rotational constants for all these species have been implemented in the MADEX code (Cernicharo 2012) in order to work for their detection and analysis in interstellar and circumstellar sources.

The HCCNC and HNCCC isomers were previously detected towards TMC-1 by Kawaguchi et al. (1992a,b) and in IRC+10216 by Gensheimer (1997a,b). A detailed study of these two species in L1544, including their relative abundances, formation paths, and comparison with the abundances observed in TMC-1 has been conducted by Vastel et al. (2018) based on observations in the λ 3 mm domain.

The derived line parameters for the HCCNC and HNCCC transitions observed in TMC-1 are given in Table A.1. Selected lines are shown in Fig. 1. The deuterated counterparts DNCCC and DCCNC, together with the three ^{13}C substitutions of HCCNC, have also been detected for the first time in space. Its derived line parameters are given in Table A.1 (see also Fig. 1). Improved rotational constants for DNCCC, H^{13}CCNC, HC^{13}CNC, and HCCN^{13}C were obtained from the observed frequencies. They are given in Appendix A. The isotopic abundance ratios of the HC_3N isomers are discussed in Appendix B.

Assuming a TMC-1 source size of 40″ and that the rotational temperature of the observed transitions is identical to the kinetic temperature (10 K), we derive N(HNCCC) = (5.2 ± 0.3) × 10^{11} cm^{-2}, and N(HCCNC) = (3.0 ± 0.3) × 10^{12} cm^{-2}. We can check the validity of the assumed rotational temperature by adopting for the isomers the same collisional rates of HC_3N (Wernli et al. 2007), and a value of (4–10) × 10^4 cm^{-3} for the H_2 volume density, in the large velocity gradient (LVG) module integrated in MADEX (Cernicharo 2012). For the lowest value of the H_2 density, the derived excitation temperatures for the J = 4–3 and 5–4 transitions are 9.5 and 8.2 K for HCCNC, whereas they are 10 and 7 K for HNCCC. For $n(H_2)$ = 10^5 cm^{-3}, these rotational transitions will have excitation temperatures very close to 10 K. For HC_3N, we also performed LVG calculations leading to derived excitation temperatures very close to 10 K for the J = 4–3 and 5–4 transitions. However, these HC_3N transitions exhibit line opacity problems due to the high abundance of this molecule in TMC-1. The very weak hyperfine components F = 4–4 and F = 3–3 of the J = 4–3 transition, and the F = 5–5 and F = 4–4 of the J = 5–4 transition, were detected. We used those components to derive $N(HC_3N)$ = (2.3 ± 0.2) × 10^{14} cm^{-2}, which is a value 1.5 times larger than the one obtained using only the strongest hyperfine components of the observed rotational transitions. We can also estimate the column density of cyanoacetylene by using its ^{13}C isotopologues (see Table B.2) and a ^{12}C/^{13}C abundance ratio of 93 ± 10 (derived from all isotopologues of HC_5N, see Appendix B). In this case, the result is $N(HC_3N)$ = (1.9 ± 0.2) × 10^{14} cm^{-2}. Our value for the isotopic abundance ratio agrees rather well with the one derived by Takano et al. (1998) in the same source. The derived column densities for HNCCC, HCCNC, and HC_3N in TMC-1 (see

[2] https://nanocosmos.iff.csic.es/
[3] http://www.iram.fr/IRAMFR/GILDAS

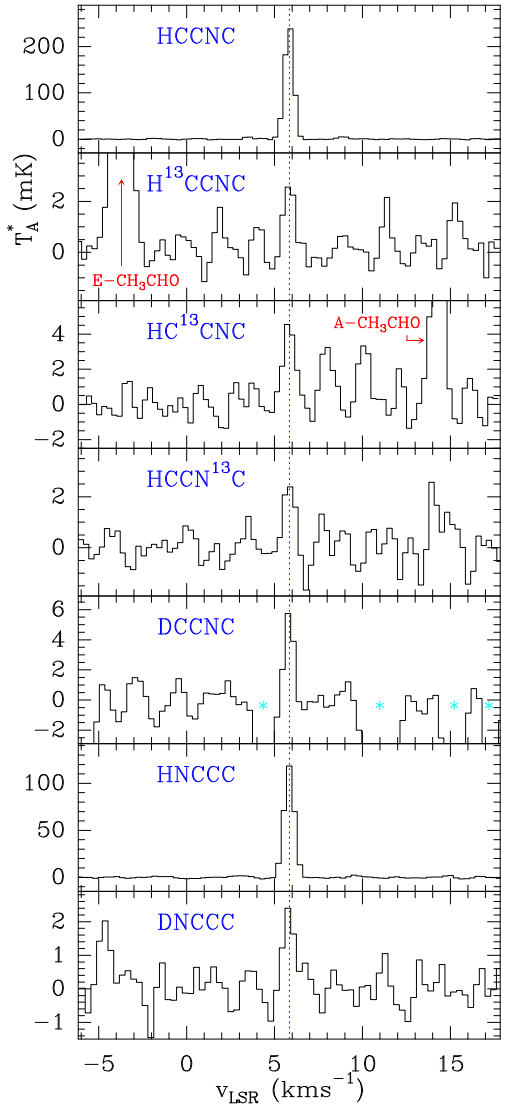

Fig. 1. J = 4–3 transition of HNCCC, HCCNC, and some of their isotopologues, observed towards TMC-1. The abscissa corresponds to the local standard of rest velocity in km s^{-1}. Frequencies and intensities for the observed lines are given in Table A.1. The ordinate is the antenna temperature corrected for atmospheric and telescope losses in mK. Cyan stars indicate the position of ghost negative features in the spectra produced by the frequency switching observation mode. Other spectral features arising from other molecular species, or otherwise unidentified, are labeled in the different panels.

Table 1) are in reasonable agreement with those obtained previously (Kawaguchi et al. 1992a,b; Takano et al. 1998). We note that our assumed rotational temperatures are higher than those reported in the literature (5–7 K), but the differences in the estimated column densities for optically thin lines involving energy levels between 5–8 K is is rather small. For example, for $T_{\rm rot}$ = 5 K and N(HNCCC) = 10^{11} cm^{-2}, the expected brightness intensity for its J = 4–3 transition is ~43.5 mK, while for $T_{\rm rot}$ = 10 K, it is 50.4 mK.

The Q-band survey of IRC+10216 carried out with the Yebes 40m also reached an unprecedented sensitivity, which has allowed the detection of new molecular species such as MgC_3N and MgC_4H (Cernicharo et al. 2019), and of previously undetected vibrational excited states of abundant species such as HC_7N and HC_9N (Pardo et al. 2020). In these data, we find two transitions of HNCCC and HCCNC, with their observed line

Table 1. Column densities [(a)] and abundance ratios for the isomers of HC_3N and HC_5N towards TMC-1 and IRC+10216.

Molecule	TMC-1	IRC+10216
$N(HC_3N)$	$(2.3\pm0.2)\times10^{14}$	$(4.5\pm0.2)\times10^{14}$
N(HCCNC)	$(3.0\pm0.3)\times10^{12}$	$(1.1\pm0.1)\times10^{12}$
N(HNCCC)	$(5.2\pm0.3)\times10^{11}$	$(3.4\pm0.2)\times10^{11}$
$N(HC_5N)$	$(1.8\pm0.2)\times10^{14}$	$(4.2\pm0.4)\times10^{14}$ [(b)]
$N(HC_4NC)$	$(3.0\pm0.7)\times10^{11}$	$\leq2.1\times10^{11}$
$N(HNC_5)$	$\leq1.5\times10^{11}$	$\leq1.1\times10^{11}$
$N(HC_7N)$	$(6.4\pm0.2)\times10^{13}$	$(1.9\pm0.2)\times10^{14}$ [(c)]
$N(HC_6NC)$	$\leq9.0\times10^{10}$	$\leq2.0\times10^{11}$
$N(HC_3N)/N$(HCCNC)	77.0 ± 8.0	392 ± 22
$N(HC_3N)/N$(HNCCC)	442.0 ± 70.0	1305 ± 45
N(HCCNC)/N(HNCCC)	5.8 ± 1.0	4.0 ± 0.9
$N(HC_5N)/N(HC_4NC)$	600 ± 70.0	≥2000
$N(HC_5N)/N(HNC_5)$	≥1200	≥3800
$N(HC_4NC)/N(HNC_5)$	≥2	≥1.9
$N(HC_7N)/N(HC_6NC)$	≥710.0	≥950
$N(HC_3N)/N(HC_5N)$	1.3 ± 0.2	1.1 ± 0.2
$N(HC_5N)/N(HC_7N)$	2.8 ± 0.3	2.2 ± 0.5

Notes. [(a)]All column densities are given in units of cm^{-2}. [(b)]For IRC+10216, we adopted the value derived by Pardo et al. (2020), which corresponds to the gas component with $T_{\rm rot}$ = 10.1 K. A second component, with similar column density, was found for high-J levels with a $T_{\rm rot}$ = 24.5 K. [(c)]For IRC+10216, we adopted the value derived by Pardo et al. (2020), which corresponds to the gas component with $T_{\rm rot}$ = 16.8 K. A second component, with a column density 2.5 lower, was found for high-J levels with a $T_{\rm rot}$ = 31.6 K.

parameters, which are given together with those of HC_3N and their isotopologues in Table A.2. The isotopologues of the isomers are, however, below the sensitivity limit of the data. We performed an LVG model to derive the column densities of the three HC_3N isomers from the observations. The results are given in Table 1. To avoid line opacity effects, the column density of HC_3N has been derived from the observed intensities of its three ^{13}C isotopologues using an isotopic abundance ratio of 45 (Cernicharo et al. 2000).

3.2. The isomers of HC_5N. Detection of HC_4NC

HC_5N has different isomers shown in Fig. C.1. The most stable one, after HC_5N, is HC_4NC (see Appendix C). Both of them could be formed in TMC-1 through the dissociative recombination of the cation HC_5NH^+, recently detected in TMC-1 by Marcelino et al. (2020). Through its similarity to HC_3N and HNCCC, the isomer HNC_5 could also be formed in the dissociative recombination of HC_5NH^+. While HC_4NC has been observed in the laboratory (Botschwina et al. 1998) and precise rotational frequencies are available from the Cologne Database for Molecular Spectroscopy (CDMS) catalogue (Müller et al. 2005) or from the MADEX code (Cernicharo 2012), no laboratory data are available for HNC_5. Nevertheless, we estimated, using ab initio calculations, its rotational constants and searched for this species in TMC1 and IRC+10216.

Five lines of HC_4NC were detected towards TMC-1 (see Fig 2). This is the first time that this species has been detected in space. From the rotational diagram obtained with its observed line intensities, we derived $T_{\rm rot}$ = 9.8 ± 0.9 K, and $N(HC_4NC) = (3.0\pm0.7)\times10^{11}$ cm^{-2}. In order to compare the derived column density with that of the most stable isomer, HC_5N, we used the observed intensities of this last species (see Table B.3) to build another rotational diagram. We obtained

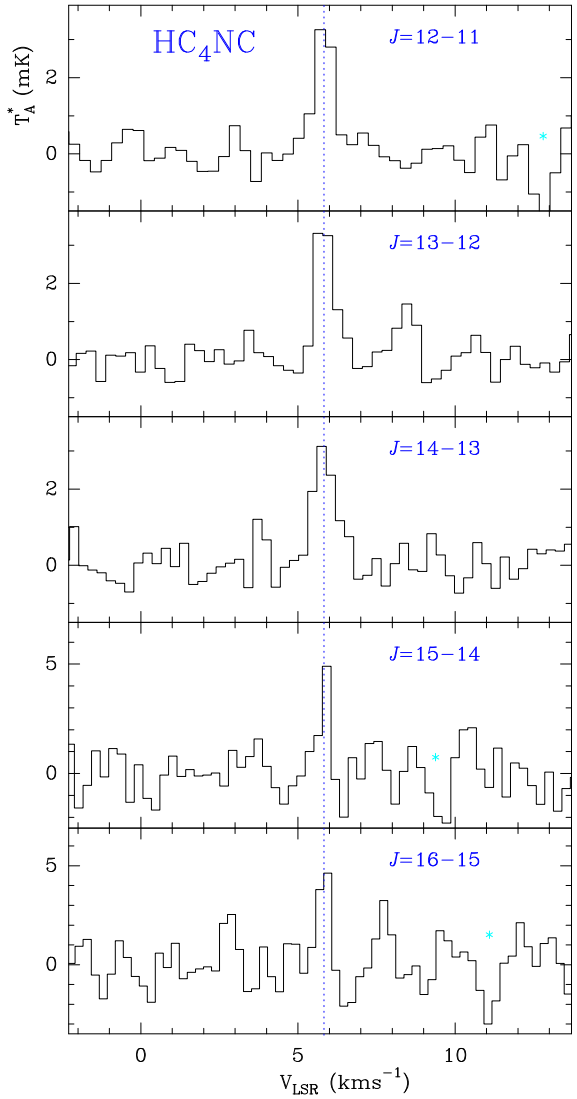

Fig. 2. Observed lines of HC_4NC found in the 31–50 GHz frequency range towards TMC-1. The abscissa corresponds to the local standard of rest velocity in km s^{-1}. Frequencies and intensities for the observed lines are given in Table 2. The ordinate is the antenna temperature corrected for atmospheric and telescope losses in mK. The $J = 17-16$ line is not detected within a 3σ level of 5.7 mK. Spectral resolution is 38.1 kHz.

$T_{\rm rot} = 8.6 \pm 0.2$ K, and $N(HC_5N) = (1.8 \pm 0.2) \times 10^{14}$ cm^{-2} (corrected for line opacity effects, see Appendix B). Hence, the HC_5N/HC_4NC abundance ratio in TMC-1 is ~600. Using the observed frequencies of HC_4NC in TMC-1 and those obtained in the laboratory (Botschwina et al. 1998), we improved the rotational constants of this species (see Appendix A).

We searched for the lines of HC_4NC towards IRC+10216 without success. By averaging all the data from the expected line positions within the *Q*-band, we derived a column density upper limit of 2×10^{11} cm^{-2}. Using the same dataset, the column density of HC_5N was recently derived as $(4.2 \pm 0.4) \times 10^{14}$ cm^{-2} (Pardo et al. 2020). Hence, in this carbon-rich circumstellar envelope, the HC_5N/HC_4NC abundance ratio is ≥2000.

Precise rotational constants were estimated through our ab initio calculations for HNC_5 (scaled values $B_0 = 1358.8 \pm 1.0$ MHz, $D_0 \sim 32$ Hz; see Appendix C). Although slightly asymmetrical, it is a quasi-linear species (see Appendix C) such that we could expect the J_{0J} series of lines to be in harmonic relation. The $K = 1$ lines could be at an energy too high to be detected in TMC1. We searched for such an harmonic pattern around ±100 MHz of the predicted line frequencies without success. Using the dipole moment we derived from our calculations, we get $N(HNC_5) \leq 1.5 \times 10^{11}$ cm^{-2} and $\leq 1.1 \times 10^{11}$ cm^{-2} towards TMC-1 and IRC+10216, respectively.

Table 2. Observed line parameters of HCCCCNC in TMC-1.

J_u	$\nu_{\rm obs}$ [a] (MHz)	T_A^* [b] (mK)	Δv [c] (kms^{-1})	$\int T_A^* dv$ [d] (mK kms^{-1})
12	33628.151 ± 0.010	3.6 ± 0.5	0.71 ± 0.12	2.68 ± 0.3
13	36430.429 ± 0.010	3.8 ± 0.5	0.66 ± 0.09	2.68 ± 0.3
14	39232.730 ± 0.010	3.1 ± 0.6	0.85 ± 0.12	2.76 ± 0.3
15	42035.040 ± 0.010	3.7 ± 1.0	0.47 ± 0.14	2.08 ± 0.4
16	44837.295 ± 0.010	4.9 ± 1.2	0.42 ± 0.19	2.24 ± 0.5

Notes. [a]Observed frequencies for a $v_{\rm LSR}$ of 5.83 km s^{-1}. The $J = 17-16$ line has not been detected within a 3σ level of 5.7 mK. [b]Antenna temperature in mK. [c]Linewidth at half intensity derived by fitting a Gaussian line profile to the observed transitions (in kms^{-1}). [d]Integrated line intensity in mK kms^{-1}.

3.3. The isomers of HC_7N

HC_7N has 17 rotational transitions within the frequency range of our *Q*-band data. All of them have been detected in TMC1 and in IRC+10216. For the latter source, the data were presented and analyzed by Pardo et al. (2020); the derived HC_7N column density is given in Table 1. From the TMC1 data (see Table B.3), we built a rotational diagram that gives the following results: $T_{\rm rot} = 7.6 \pm 0.1$ K and $N(HC_7N) = (6.4 \pm 0.4) \times 10^{13}$ cm^{-2}.

The most stable isomer of HC_7N is HC_6NC, which was previously observed in the laboratory by Botschwina et al. (1998). We searched for its lines towards both sources without success. The derived upper limits, which are based on a stacking of the $J = 28$–27 up to $J = 31$–30 transitions, are given in Table 1.

4. Discussion

The chemistry of HC_3N isomers in cold dense clouds has been discussed by Osamura et al. (1999) and Vastel et al. (2018). In the scenario depicted by these authors, the main formation route to the HC_3N isomers relies on the dissociative recombination of HC_3NH^+. The rate constant of this reaction has been measured, using the deuterated variant of the ion, by Geppert et al. (2004). Calculations by Osamura et al. (1999) indicate that rearrangement is possible so that the various linear or nearly-linear isomers of HC_3N, that is, HNC_3, HCCNC, and HCNCC, can be formed. There is some experimental information on the different fragments that are formed (Geppert et al. 2004), but precise branching ratios for the different exit channels are not known and introduce important uncertainties when modeling the chemistry of HC_3N isomers. The chemical models constructed for TMC-1 (Osamura et al. 1999) and for L1544 (Vastel et al. 2018) reproduce quite well the observed abundances of HC_3N isomers, although they tend to overestimate the abundances of HNC_3 and HCCNC with respect to HC_3N. In these models, the most stable isomer, HC_3N, is also formed through neutral-neutral reactions, while the different metastable isomers are mostly formed through dissociative recombination of HC_3NH^+ and, to a lesser extent, of its less stable isomer $HCCNCH^+$. The higher abundance observed for the isomer HCCNC with respect

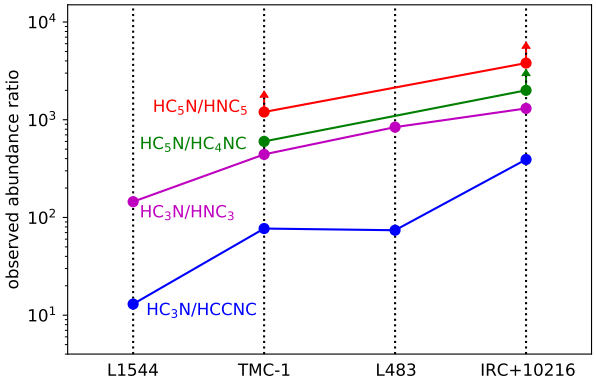

Fig. 3. Observed abundance ratios between isomers of HC_3N and HC_5N in different molecular sources. Values for TMC-1 and IRC+10216 are from this study, for L1544 from Vastel et al. (2018), and for L483 from Agúndez et al. (2019).

to HNC_3 is explained in terms of a higher reactivity of the latter isomer with neutral H and C atoms (Osamura et al. 1999). By way of an analogy with HC_3N, the main source of HC_5N and its isomers is most likely the dissociative recombination of HC_5NH^+, recently detected in TMC-1 (Marcelino et al. 2020). However, branching ratios for the formation of the different isomers HC_5N, HC_4NC, and HNC_5 are unknown.

Looking at how the relative abundances of HC_3N and HC_5N isomers behave in different sources can provide clues on the underlying chemical processes. In Fig. 3, we compare the abundance ratios between HC_3N isomers derived here for TMC-1 and IRC+10216 with those obtained in the molecular clouds L1544 and L483. It can be seen that the $HC_3N/HCCNC$ and HC_3N/HNC_3 ratios observed in TMC-1 are similar to those seen in the Class 0 molecular cloud L483, although they are higher than those derived in the starless core L1544 and lower than the values in the C-star envelope IRC+10216. The change in these abundance ratios may be related to the temperature of the source. The low temperature of the starless core L1544 seems to favor the formation of metastable isomers while these are less efficiently formed in the warmer ejecta of IRC+10216. Indeed, as temperature increases, the presence of high-energy isomers is less favorable because chemical reactions, including isomerization, are expected to favor the most stable isomer. The same is expected to be true of isotopic fractionation. For example, in TMC-1, the isotopologue $HCC^{13}CN$ is twice as abundant as $H^{13}CCCN$ and $HC^{13}CCN$ (see also Takano et al. 1998), whereas, in the case of HCCNC, its $HC^{13}CNC$ isotopologue is 1.8 times more abundant than $H^{13}CCNC$ and $HCCN^{13}C$ (see Table B.1). A slight overabundance of $HCCCC^{13}CN$ with respect to the other four ^{13}C isotopologues of HC_5N has also been observed (see Appendix B). These kinds of isotopic anomalies have been also seen for HC_3N in other cold dense clouds (Araki et al. 2016; Taniguchi et al. 2017; Agúndez et al. 2019), but they are not seen in IRC+10216.

The column densities and abundance ratios derived for the isomers of HC_3N, HC_5N, and HC_7N in TMC-1 and IRC+10216 are summarized in Table 1. The abundance ratios given in Table 1 (see also Fig. 3), suggest a trend in which the relative abundance of metastable isomers decreases as we move to larger molecular sizes. In TMC-1, we have $N(HCN)/N(HNC) \simeq 1$, $N(HC_3N)/N(HCCNC) \simeq 77$, $N(HC_3N)/N(HNC_3) \simeq 442$, $N(HC_5N)/N(HC_4NC) \sim 600$, and $N(HC_7N)/N(HC_6NC) \geq 710$. These ratios are increased by a factor of ~4–5 in IRC+10216. This suggests that metastable isomers of longer carbon chains will be hardly detectable in these sources.

Acknowledgements. The Spanish authors thank Ministerio de Ciencia e Innovación for funding support through project AYA2016-75066-C2-1-P. We also thank ERC for funding through grant ERC-2013-Syg-610256-NANOCOSMOS. MA and CB thanks Ministerio de Ciencia e Innovación for Ramón y Cajal grant RyC-2014-16277 and Juan de la Cierva grant FJCI-2016-27983.

References

Agúndez, M., Marcelino, N., & Cernicharo, J. 2018, ApJ, 861, L22
Agúndez, M., Marcelino, N., Cernicharo, J., et al. 2019, A&A, 625, A147
Araki, M., Takano, S., Sakai, N., et al. 2016, ApJ, 833, 291
Bizzocchi, L., Degli Esposti, C., & Botschwina, P. 2004, J. Mol. Spectr., 225, 145
Botschwina, P., Heyl, A., Chen, W., et al. 1998, J. Chem. Phys., 109, 3108
Cernicharo, J. 1985, Internal IRAM report (Granada: IRAM)
Cernicharo, J., Kahane, C., Guélin, M., & Gómez-Gónzalez, J. 1988, A&A, 189, L1
Cernicharo, J., Guélin, M., & Kahane, C. 2000, A&AS, 142, 181
Cernicharo, J. 2012, EAS Pub. Ser., 58, 251, https://nanocosmos.iff.csic.es/?page_id=1619
Cernicharo, J., Daniel, F., Castro-Carrizo, A., et al. 2013, ApJ, 778, L25
Cernicharo, J., Cabezas, C., Pardo, J. R., et al. 2019, A&A, 630, L2
Cernicharo, J., Marcelino, N., Pardo, J. R., et al. 2020, A&A, 641, L9
Chen, W., Bocquet, R., Wlodarczak, G., & Boucher, D. 1991, Int. J. Infrared Millimeter Waves, 12, 987
Cížek, J. 1969, in Advances in Chemical Physics, ed. P. C. Hariharan (New York: Wiley Interscience), 14, 35
Creswell, R. A., & Winnewisser, G. 1977, J. Mol. Spectr., 65, 420
Cuadrado, S., Goicoechea, J. R., Roncero, O., et al. 2016, A&A, 596, L1
De Zafra, R. L. 1971, ApJ, 170, 165
Fayt, A., Vigouroux, C., Willaert, F., et al. 2004, J. Mol. Struct., 695–696, 295
Frisch, M. J., Trucks, G. W., Schlegel, H. B., et al. 2013, Gaussian, 09, rev. D.01
Gensheimer, P. D. 1997a, Astrophys. Space Sci., 251, 199
Gensheimer, P. D. 1997b, ApJ, 479, L75
Geppert, W. D., Ehlerding, A., Hellberg, F., et al. 2004, ApJ, 613, 1302
Gordy, W., & Cook, R. L. 1984, Microwave Molecular Spectra, Chapter V (New York: Wiley)
Gronowski, M., & Kołos, R. 2006, Chem. Phys. Let., 428, 245
Gronowski, M., & Kołos, R. 2007, J. Mol. Struct., 834–836, 102
Guarnieri, A., Hinze, R., Krüger, M., & Zerbe-Foese, H. 1992, J. Mol. Spectr., 156, 39
Hacar, A., Bosman, A. D., & van Dishoeck, E. F. 2020, A&A, 635, A4
Hirahara, Y., Ohsihima, Y., & Endo, Y. 1993, ApJ, 403, L83
Huckauf, A., Guarnieri, A., Lentz, D., & Fayt, A. 1998, J. Mol. Spectr., 188, 109
Kaifu, N., Ohishi, M., Kawaguchi, K., et al. 2004, PASJ, 56, 69
Kawaguchi, K., Ohishi, M., Ishikawa, S.-I., & Kaifu, N. 1992a, ApJ, 386, L51
Kawaguchi, K., Takano, S., Ohishi, M., Ishikawa, S.-I., et al. 1992b, ApJ, 396, L49
Krüger, M., Stahl, W., & Dreizler, H. 1992, J. Mol. Spectr., 158, 298
Mallinson, P. D., & De Zafra, R. L. 1978, Mol. Phys., 36, 872
Marcelino, N., Agúndez, M., Tercero, B., et al. 2020, A&A in press, https://doi.org/10.1051/0004-6361/202039251
Mbosei, L., Fayt, A., & Dréan, P. 2000, J. Mol. Struct., 517, 271
Møller, C., & Plesset, M. S. 1936, Phys. Rev., 46, 618
Müller, H. S. P., Schlöder, F., Stutzki, J., & Winnewisser, G. 2005, J. Mol. Struct., 742, 215
Osamura, Y., Fukuzawa, K., Terzieva, R., & Herbst, E. 1999, ApJ, 519, 697
Pardo, J. R., Cernicharo, J., & Serabyn, E. 2001, IEEE Trans. Antennas Propag., 49, 12
Pardo, J. R., Bermúdez, C., Cabezas, C., et al. 2020, A&A, 640, L13
Spahn, H., Müller, H. S. P., & Giesen, T. 2008, Chem. Phys., 346, 132
Tack, L. M., & Kukolich, S. G. 1983, J. Chem. Phys., 78, 6512
Takano, S., Masuda, A., Hirahara, Y., et al. 1998, A&A, 329, 1156
Taniguchi, K., Ozeki, H., Saito, M., et al. 2016, ApJ, 817, 147
Taniguchi, K., Ozeki, H., & Saito, M. 2017, ApJ, 846, 46
Taquet, V., Wirström, E. S., Charnley, S. B., et al. 2017, A&A, 607, A20
Thorwirth, S., Müller, H. S. P., & Winnewisser, G. 2000, J. Mol. Spectr., 204, 133
Thorwirth, S., Müller, H. S. P., & Winnewisser, G. 2001, PCCP, 3, 1236
Vastel, C., kawaguchi, K., Quénard, D., et al. 2018, MNRAS, 474, L76
Wernli, M., Wiesenfeld, L., Faure, A., & Valiron, P. 2007, A&A, 475, 391
Xue, C., Willis, E. R., Loomis, R. A., et al. 2020, ApJ, 900, L9
Yamada, K. M. T., Moravec, A., & Winnewisser, G. 1995, Z. Naturforsch, 50a, 133

Appendix A: Improved rotational constants for the isotopologues of HNCCC and HCCNC and for HC_4NC

While the rotational spectrum of HCCNC was already measured in the laboratory up to $J_{up} = 33$ by Guarnieri et al. (1992), only the $J = 1$–0 rotational transition of its ^{13}C isotopologues has been measured so far (Krüger et al. 1992). Predictions for the frequencies of their rotational transitions have been obtained by initially assuming a distortion constant similar to that of the main isotopologue. This allows us to derive frequencies with uncertainties of 50–140 kHz for lines in the 31–50 GHz frequency interval. The $J = 4$–3 and 5–4 lines of $H^{13}CCNC$, $HC^{13}CNC$, and $HCCN^{13}C$ were easily detected in TMC-1 and their frequencies have been obtained with an accuracy better than 10 kHz assuming a v_{LSR} for the source of 5.83 km s^{-1} (see Sect. 3). The derived line parameters are given in Table A.1 and the spectra are shown in Fig. 1. The observed line parameters for these species in IRC+10216 are given in Table A.2

For the deuterated species, DCCNC, the rotational spectrum up to $J_{up} = 51$ was measured by Huckauf et al. (1998). Its rotational lines within the Q-band are predicted with a high level of accuracy (the derived line parameters are given in Table A.1, see Fig. 1). For DNCCC, only the $J = 1$–0 and 2–1 lines were measured in the laboratory by Hirahara et al. (1993). In our study, we detected the $J = 4$–3 and 5–4 lines in TMC-1 and, again, we determined their central frequencies with an accuracy better than 10 kHz. The derived line parameters are also given in Table A.1 and the corresponding spectra are shown in Fig. 1.

As a next step, by combining the laboratory data (Krüger et al. 1992; Hirahara et al. 1993) with the frequencies derived towards TMC-1, we obtained a new set of rotational constants for DNCCC, $H^{13}CCNC$, $HC^{13}CNC$, and $HCCN^{13}C$. The hyperfine structure parameters, nuclear quadrupole, spin-rotation, and spin-spin constants have been fixed to the values derived from laboratory data, that is, we fitted only the rotational and the distortion constants. The results are provided in Table A.3. With this new set of constants, the frequencies of the isotopologues can be predicted with accuracies better than 20 kHz at rest frequencies up to 80 GHz, and better than 100 kHz for rest frequencies up to 130 GHz ($J_{up} = 15$).

For HC_4NC, the laboratory data cover lines from $J = 3$–2 up to $J = 6$–5 (Botschwina et al. 1998). The rotational lines observed in TMC1 add five more rotational transitions, from $J = 12$–11 up to $J = 16$–15. By fitting the laboratory and astrophysical lines, a new set of rotational constants were obtained for this species (see Table A.3). The best improvement is obtained for the distortion constant, D_0, which is derived to be 32.8 ± 0.4 Hz, compared with the laboratory value of 34.3 ± 0.9 Hz. Predictions using the new constants have an accuracy better than 20 kHz up to 70 GHz, and better than 100 kHz up to 115 GHz ($J = 41$–40).

Table A.1. Observed line parameters of HNCCC and HCCNC in TMC-1.

Molecule	J_u–J_l	ν_{obs} [a] (MHz)	T_A^* (mK)	Δv [b] (kms^{-1})	$\int T_A^* dv$ [c] (mK kms^{-1})	σ [d] (mK)
HNCCC	4–3	37346.541(10)	118.7	0.70(1)	88.8(10)	0.6
HNCCC	5–4	46683.061(10)	121.2	0.57(1)	73.5(10)	1.5
DNCCC	4–3	35204.594(10)	2.4	0.76(9)	1.95(06)	0.5
DNCCC	5–4	44005.628(10)	3.2	0.46(9)	1.64(07)	1.1
HCCNC	4–3	39742.549(10)	249.2	0.62(1)	164.7(10)	0.8
HCCNC	5–4	49678.075(10)	224.6	0.58(1)	138.4(10)	1.9
DCCNC	4–3	36786.182(10)	6.1 [e]	0.58(9)	3.74(90)	0.7
DCCNC	5–4	45982.625(10)	9.9	0.60(8)	6.38(30)	1.1
$H^{13}CCNC$	4–3	38504.813(10)	2.8	0.68(9)	2.03(30)	0.6
$H^{13}CCNC$	5–4	48130.916(10)	4.5	0.45(9)	2.50(80)	1.7
$HC^{13}CNC$	4–3	39595.406(10)	4.7	0.80(9)	3.97(30)	0.7
$HC^{13}CNC$	5–4	49494.139(07)	≤4.5 [f]			1.5
$HCCN^{13}C$	4–3	38438.864(10)	2.7	0.68(9)	1.92(40)	0.6
$HCCN^{13}C$	5–4	48048.449(10)	5.4	0.45(9)	2.58(70)	1.8
$HCC^{15}NC$	4–3	39557.751(50)	≤2.2 [f]			0.7

Notes. [a]Observed frequencies for a v_{LSR} of 5.83 km s^{-1}. For all entries, values between parentheses represent the uncertainty in units of the last digit. [b]Linewidth at half intensity derived by fitting a Gaussian line profile to the observed transitions (in kms^{-1}). [c]Integrated line intensity in mK km s^{-1}. [d]The sensitivity of the data (root mean square error) has been derived from a baseline to the each line in a velocity window −6.2 to 17.8 km s^{-1} (in mK). [e]Blended with a negative feature produced by the frequency switching observing mode. [f]3σ upper limit. Observed frequency has been replaced by the predicted frequency.

Table A.2. Observed line parameters for HNCCC, HCCNC, and HC_3N in IRC+10216.

Molecule	j_u–j_l	ν_{obs} [a] (MHz)	$\int T_A^* dv$ [b] (K kms^{-1})
HNCCC	4–3	37346.448(50)	0.064(07)
HNCCC	5–4	46683.020(80)	0.077(07)
HCCNC	4–3	39742.549(30)	0.075(04)
HCCNC	5–4	49678.155(50)	0.078(06)
HCCCN	4–3	36392.327(10)	21.21(15)
HCCCN	5–4	45490.311(10)	24.20(15)
H^{13}CCCN	4–3	35267.369(20)	0.620(08)
H^{13}CCCN	5–4	44084.175(50)	0.959(07)
HC^{13}CCN	4–3	36237.909(50)	0.621(08)
HC^{13}CCN	5–4	45297.243(50)	0.913(07)
HCC^{13}CN	4–3	36241.427(50)	0.605(08)
HCC^{13}CN	5–4	45301.689(50)	1.046(08)

Notes. [a]Observed frequencies for a v_{LSR} of -26.5 km s^{-1} (Cernicharo et al. 2000). For all entries, values between parentheses represent the uncertainty in units of the last digit. [b]Integrated line intensity in K kms^{-1}.

Table A.3. New rotational and distortion constants for some isotopologues of HNCCC and HCCNC and for HC_4NC.

Molecule	B_0 [a] (MHz)	D_0 (kHz)	J_{max}	σ [b] (kHz)
DNCCC	4400.5944(4)	0.63(9)	5	1.7
H^{13}CCNC	4813.1187(6)	0.54(4)	5	2.5
HC^{13}CNC	4949.4462(3)	0.64(4)	4	1.0
HCCN^{13}C	4804.8737(5)	0.56(3)	5	13.8
HCCCCNC [c]	1401.18216(6)	0.0328(4)	16	7.0

Notes. [a]Values between parentheses represent the uncertainty in units of the last digit. [b]Standard deviation of the fit. [c]The fitted value for eQq is 0.97(3) MHz.

Appendix B: HC_3N, HC_5N, and HC_7N column densities and isotopic abundance ratios

Rest frequencies for the ^{13}C isotopologues of HC_3N were obtained by fitting all the observed rotational transitions in the laboratory (Creswell & Winnewisser 1977; Mallinson & De Zafra 1978; Thorwirth et al. 2001). For the ^{15}N isotopologue, the measured frequencies from these references and those from Fayt et al. (2004) have been used to derive its rotational parameters.

For DC_3N, all available laboratory data were used to derive its rotational parameters (Mallinson & De Zafra 1978; Tack & Kukolich 1983; Spahn et al. 2008). The main isotopologue has been extensively observed in the laboratory up to $J = 89$ (De Zafra 1971; Mbosei et al. 2000; Creswell & Winnewisser 1977; Chen et al. 1991; Yamada et al. 1995; Thorwirth et al. 2000). The derived rotational parameters were implemented in the MADEX code (Cernicharo 2012). The derived rest frequencies for the observed transitions are given in Table B.2.

For HC_5N and its ^{13}C, ^{15}N, and D isotopologues we fit the rotational transitions measured in the laboratory by Bizzocchi et al. (2004) and, again, the resulting rotational constants have been implemented in the MADEX code. The rest frequencies for the observed transitions are given in Table B.3.

Table B.1. Derived column densities for the isotopologues of HC_3N and HC_5N in TMC-1.

Species	T_{rot} [a] (K)	N [b] (cm^{-2})
HCCCN	10.0 [d]	$(2.3 \pm 0.2) \times 10^{14}$ [c]
H^{13}CCCN	10.0 [d]	$(2.5 \pm 0.2) \times 10^{12}$
HC^{13}CCN	10.0 [d]	$(2.9 \pm 0.2) \times 10^{12}$
HCC^{13}CN	10.0 [d]	$(3.6 \pm 0.2) \times 10^{12}$
DCCCN	10.0 [d]	$(3.7 \pm 0.2) \times 10^{12}$
HCCNC	10.0 [d]	$(3.0 \pm 0.2) \times 10^{12}$
H^{13}CCNC	10.0 [d]	$(4.1 \pm 0.4) \times 10^{10}$
HC^{13}CNC	10.0 [d]	$(7.3 \pm 0.4) \times 10^{10}$
HCCN^{13}C	10.0 [d]	$(4.0 \pm 0.4) \times 10^{10}$
DCCNC	10.0 [d]	$(1.0 \pm 0.3) \times 10^{11}$
HNCCC	10.0 [d]	$(5.2 \pm 0.3) \times 10^{11}$
DNCCC	10.0 [d]	$(1.2 \pm 0.2) \times 10^{10}$
HC_5N	8.6 ± 0.2	$(1.8 \pm 0.2) \times 10^{14}$ [c]
H^{13}CCCCCN	7.3 ± 0.2	$(1.8 \pm 0.2) \times 10^{12}$
HC^{13}CCCCN	6.0 ± 0.1	$(2.1 \pm 0.2) \times 10^{12}$
HCC^{13}CCCN	6.6 ± 0.2	$(2.0 \pm 0.4) \times 10^{12}$
HCCC^{13}CCN	7.8 ± 0.4	$(1.7 \pm 0.3) \times 10^{12}$
HCCCC^{13}CN	7.3 ± 0.2	$(2.1 \pm 0.2) \times 10^{12}$
HCCCCC^{15}N	8.7 ± 1.4	$(4.6 \pm 1.0) \times 10^{11}$
DCCCCCN	7.3 ± 0.4	$(2.2 \pm 0.4) \times 10^{12}$
HC_7N	7.6 ± 0.1	$(6.4 \pm 0.4) \times 10^{13}$

Notes. [a]Derived rotational temperature in K from the data in Tables B.2 and B.3. [b]Derived column density in cm^{-2}. [c]Corrected for line opacity effects (see text). [d]Adopted value (see text).

In order to derive column densities for all isotopologues of HC_3N, HNCCC, and HCCNC, for which only two rotational lines ($J = 4$–3 and 5–4) have been observed in TMC-1, we assumed that the molecule is thermalized at a kinetic temperature of the cloud of 10 K and a source radius of 40″ (see Sect. 3.1). The derived column densities are given in Table B.1 and the line parameters for the HC_3N rotational transitions used for this analysis are given in Table B.2. We confirm a previous result of Takano et al. (1998) concerning the overabundance of HCC^{13}CN with respect to the other two ^{13}C isotopologues. These authors analyzed the chemical processes that could lead to the enriched abundance for this particular isotopologue and concluded that it is produced during the formation process of HC_3N – and not through a reaction of $^{13}C^+$ with HC_3N. This effect also shows up in HCCNC, for which its HC^{13}CNC isotopologue is 1.8 times more abundant than H^{13}CCNC and HCCN^{13}C (see Table B.1). We conclude, hence, that the carbon-13 attached to the nitrogen atom has a clear overabundance with respect to the other isotopologues of HCCCN and HCCNC.

For IRC+10216, the isotopic abundances have been discussed in detail by Cernicharo et al. (2000) who derived a ^{12}C/^{13}C value of 45 ± 3. It should be pointed out that for the three isotopologues, the intensities of the $J = 4$–3, and 5–4 transitions differ by less than 2% and 5%, respectively (see Table A.2). Hence, no fractionation effects are observed for HC_3N in IRC+10216.

For HC_5N, we observed seven lines of each one of its isotopologues towards TMC-1. Consequently, a rotational diagram can be built for each one of them (see Table B.3). The derived rotational temperatures and column densities are given in Table B.1. The rotational diagram provides a colum density of $(9.0 \pm 0.1) \times 10^{13}$ cm^{-2}, which has to be considered as a lower limit because the lines show opacity effects. The weak hyperfine components corresponding to $F = J_u - J_u$ and $J_l - J_l$, which are placed at ~1.5–2 MHz from the blended three strongest hyperfine components $\Delta F = 1$, are detected for $J_u = 12$ up to 16. As an example, the transition $J = 16-15$ has three strong hyperfine components separated by a few kHz and representing a total line strenght of 47.875. The two weak hyperfine components have an added line strenght of 0.125. The theoretical integrated line intensity could have a ratio of 383 between the strong and weak hyperfine components, while the observed value is 153 (see Table B.3). For the $J_u = 12$ transition, the expected ratio is 215, while the observed value is 100.4. Therefore, in order to have a good estimate of the main isotopologue column density, we have to correct the derived column density from the strongest hyperfine components by a factor of ~2. Our best estimate for the HC_5N column density is, therefore, $(1.8 \pm 0.2) \times 10^{14}$ cm^{-2}.

Unlike the case of HC_3N, the ^{13}C isotopologues of HC_5N do not show any significant abundance ratio anomaly. Nevertheless, the isotopologue HCCCC^{13}CN shows, for all observed transitions, a slightly larger intensity than the other ^{13}C substitutions. In order to evaluate whether this variation is statistically relevant, we derived the integrated intensity ratios for each observed transition, taking H^{13}CCCCCN as reference. The average values of these ratios for the $J = 12$–11 up to $J = 16$–15 lines are:

HC^{13}CCCCN/H^{13}CCCCCN = 0.99 ± 0.04,
HCC^{13}CCCN/H^{13}CCCCCN = 1.03 ± 0.04,
HCCC^{13}CCN/H^{13}CCCCCN = 1.01 ± 0.04,
and
HCCCC^{13}CN/H^{13}CCCCCN = 1.15 ± 0.04.

Takano et al. (1998) reported the detection of H^{13}CCCCCN and HCCCC^{13}CN, claiming an abundance ratio of 1.3 between them. However, our more sensitive data suggest a similar abundance for all ^{13}C isotopologues, with a slightly larger abundance of 15% (within 3.5σ) for HCCCC^{13}CN. The average value for the column density derived from the five ^{13}C isotopologues is $(1.94 \pm 0.08) \times 10^{12}$ cm^{-12}. Consequently, the ^{12}C/^{13}C abundance ratio in TMC-1 is 93 ± 10, which is very close to the solar value. For the observation of two rotational lines of the five isotopologues, Taniguchi et al. (2016) obtained a similar value for the isotopic ratio, 94 ± 6. They also concluded that no significant differences do exist between the abundances of the five ^{13}C isotopologues.

Finally, we derived a N/^{15}N isotopic abundance ratio of $N(HC_5N)/N(HC_5^{15}N) = 391 \pm 85$ and a deuterium enrichment $N(HC_5N)/N(DC_5N) = 82 \pm 20$. This deuteration enrichment is similar to the one derived from HC_3N (~60), HNCCC (~43), and HCCNC (~30).

Table B.2. Observed line parameters for HC_3N and its isotopologues in TMC-1.

Molecule	J_u–J_l	F_u–F_l	ν_{rest} [a] (MHz)	T_A^* (K)	v_{LSR} [b] (kms^{-1})	Δv [c] (kms^{-1})	$\int T_A^* dv$ [d] (mK kms^{-1})	σ [e] (mK)
HCCCN	4–3	4–4	36390.8876(5)	0.444	5.81(01)	0.68(02)	0.3235(10)	0.6
HCCCN	4–3	3–2	36392.2345(5)	1.865	5.85(02)	0.65(05)	1.2943(10)	0.6
HCCCN	4–3	4–3/5–4 [e]	36392.3429(5)	2.981	5.78(02)	0.89(05)	2.8274(10)	0.6
HCCCN	4–3	3–3	36394.1777(5)	0.457	5.80(01)	0.67(02)	0.3258(10)	0.6
HCCCN	5–4	5–5	45488.8387(5)	0.385	5.81(02)	0.55(03)	0.2358(10)	1.3
HCCCN	5–4	4–3	45490.2594(5)	1.669	5.83(10)	0.66(10)	0.8865(10)	1.3
HCCCN	5–4	5–4/6–5 [e]	45490.3222(5)	2.963	5.81(10)	0.50(10)	2.0868(10)	1.3
HCCCN	5–4	4–4	45492.1107(5)	0.383	5.80(02)	0.56(03)	0.2278(10)	1.3
H^{13}CCCN	4–3	4–4	35265.9791(7)	0.005	5.98(05)	0.96(10)	0.0053(10)	0.5
H^{13}CCCN	4–3	3–2	35267.3117(7)	0.054	5.80(02)	0.73(02)	0.0415(10)	0.5
H^{13}CCCN	4–3	4–3/5–4 [e]	35267.4191(6)	0.143	5.76(02)	0.78(02)	0.1185(10)	0.5
H^{13}CCCN	4–3	3–3	35269.2342(7)	0.006	5.66(05)	0.68(10)	0.0040(10)	0.5
H^{13}CCCN	5–4 [f]		44084.1622(8)	0.188	5.82(02)	0.77(02)	0.1538(10)	1.3
HC^{13}CCN	4–3	4–4	36236.5139(7)	0.004	5.96(05)	0.54(10)	0.0025(10)	0.6
HC^{13}CCN	4–3	3–2	36237.8535(7)	0.064	5.81(03)	0.65(03)	0.1343(10)	0.6
HC^{13}CCN	4–3	4–3/5–4 [f]	36237.9619(7)	0.167	5.77(03)	0.75(03)	0.1327(10)	0.6
HC^{13}CCN	4–3	3–3	36239.7865(7)	0.006	5.75(05)	0.63(10)	0.0052(10)	0.6
HC^{13}CCN	5–4 [f]		45297.3345(7)	0.190	5.83(02)	0.76(02)	0.1532(10)	1.3
HCC^{13}CN	4–3	4–4	36240.0100(7)	0.008	5.85(04)	0.54(02)	0.0048(10)	0.6
HCC^{13}CN	4–3	3–2	36241.3514(7)	0.093	5.82(03)	0.68(02)	0.0674(10)	0.6
HCC^{13}CN	4–3	4–3/5–4 [f]	36241.4436(7)	0.239	5.75(03)	0.72(02)	0.1820(10)	0.6
HCC^{13}CN	4–3	3–3	36243.2862(7)	0.007	5.73(04)	0.64(02)	0.0050(10)	0.6
HCC^{13}CN	5–4 [f]		45301.7069(8)	0.270	5.79(01)	0.75(02)	0.2164(10)	1.3
HCCC^{15}N	4–3		35333.8879(7)	0.079	5.77(02)	0.72(02)	0.0598(10)	0.5
HCCC^{15}N	5–4		44167.2678(9)	0.096	5.79(04)	0.55(02)	0.0567(10)	1.3
DCCCN	4–3	4–4	33771.0873(3)	0.007	5.78(10)	0.78(10)	0.0060(10)	0.5
DCCCN	4–3	3–2	33772.4373(3)	0.086	5.74(02)	0.83(03)	0.0754(20)	0.5
DCCCN	4–3	4–3/5–4 [g]	33772.5477(3)	0.229	5.76(02)	0.79(03)	0.1917(20)	0.5
DCCCN	4–3	3–3	33774.3772(3)	0.003	5.86(10)	0.78(05)	0.0020(05)	0.5
DCCCN	5–4 [f]		42215.5823(9)	0.320	5.84(02)	0.78(03)	0.2653(10)	0.9

Notes. [a]Adopted rest frequencies (see text). [b]Local standard of rest velocity of the emission for the adopted rest frequency (in kms^{-1}). [c]Linewidth at half intensity derived by fitting a Gaussian line profile to the observed transitions (in kms^{-1}). [d]Integrated line intensity in K kms^{-1}. [e]The sensitivity of the data (root mean square error) has been derived from a baseline to the each line in a velocity window −6.2 to 17.8 km s^{-1} (in mK). [f]Average of the two strongest hyperfine components. [g]Average of the three strongest hyperfine components.

Table B.3. Observed line parameters for HC_5N, its isotopologues, and HC_7N in TMC-1.

Molecule	J_u–J_l [a]	ν_{rest} [b] (MHz)	T_A^* (K)	v_{LSR} [d] (kms^{-1})	Δv [e] (kms^{-1})	$\int T_A^* dv$ [c] (K kms^{-1})	σ [f] (mK)
HC_5N	12–11	31951.7764(4)	1.925	5.83(01)	0.66(01)	1.3574(10)	0.8
	F = 11–11	31953.4494(5)	0.008	5.80(04)	0.58(06)	0.0049(10)	0.8
	F = 12–12	31950.2362(5)	0.012	5.85(02)	0.69(06)	0.0086(10)	0.8
HC_5N	13–12	34614.3853(5)	1.667	5.82(01)	0.73(01)	1.2858(10)	0.5
	F = 12–12	34616.0526(5)	0.007	5.85(03)	0.63(06)	0.0045(10)	0.5
	F = 13–13	34612.8403(5)	0.009	5.77(03)	1.17(07)	0.0105(10)	0.5
HC_5N	14–13	37276.9847(6)	1.737	5.82(01)	0.66(01)	1.2282(10)	0.5
	F = 13–13	37278.6473(5)	0.005	5.78(05)	0.62(11)	0.0031(10)	0.5
	F = 14–14	37275.4357(5)	0.006	5.81(04)	0.80(10)	0.0051(10)	0.5
HC_5N	15–14	39939.5741(6)	1.769	5.84(01)	0.59(01)	1.1078(10)	0.7
	F = 14–14	39941.2326(6)	0.005	5.93(05)	0.46(06)	0.0025(10)	0.7
	F = 15–15	39938.0215(6)	0.006	5.78(02)	0.76(09)	0.0048(10)	0.7
HC_5N	16–15	42602.1527(6)	1.710	5.84(01)	0.54(01)	0.9735(10)	1.0
	F = 15–15	42603.8075(6)	0.005	5.88(05)	0.49(07)	0.0027(10)	1.0
	F = 16–16	42600.5968(6)	0.005	5.92(05)	0.63(12)	0.0037(10)	1.0
HC_5N	17–16	45264.7196(7)	1.429	5.83(01)	0.55(01)	0.8305(10)	1.3
HC_5N	18–17	47927.2743(7)	1.213	5.84(01)	0.57(01)	0.7302(10)	1.6
$H^{13}CCCCCN$	12–11	31120.0298(22)	0.034	5.85(14)	0.65(03)	0.0236(10)	1.3
$H^{13}CCCCCN$	13–12	33713.3286(24)	0.031	5.80(04)	0.74(01)	0.0246(10)	0.6
$H^{13}CCCCCN$	14–13	36306.6185(26)	0.031	5.81(06)	0.64(02)	0.0211(10)	0.6
$H^{13}CCCCCN$	15–14	38899.8989(27)	0.030	5.82(06)	0.63(01)	0.0201(10)	0.7
$H^{13}CCCCCN$	16–15	41493.1690(29)	0.028	5.82(08)	0.54(02)	0.0161(10)	0.8
$H^{13}CCCCCN$	17–16	44086.4282(30)	0.022	5.82(16)	0.56(03)	0.0131(10)	1.2
$H^{13}CCCCCN$	18–17	46679.6757(32)	0.018	5.79(19)	0.61(04)	0.0117(10)	1.3
$H^{13}CCCCCN$	19–18	49272.9109(33)	0.018	5.91(29)	0.66(06)	0.0126(10)	1.9
$HC^{13}CCCCN$	12–11	31624.3437(20)	0.039	5.88(07)	0.65(01)	0.0270(10)	0.7
$HC^{13}CCCCN$	13–12	34259.6672(21)	0.032	5.84(05)	0.71(01)	0.0239(10)	0.5
$HC^{13}CCCCN$	14–13	36894.9814(23)	0.032	5.85(06)	0.59(02)	0.0201(10)	0.6
$HC^{13}CCCCN$	15–14	39530.2857(24)	0.030	5.88(06)	0.62(02)	0.0192(10)	0.6
$HC^{13}CCCCN$	16–15	42165.5793(26)	0.026	5.87(10)	0.54(03)	0.0149(10)	0.8
$HC^{13}CCCCN$	17–16	44800.8615(27)	0.022	5.85(12)	0.48(03)	0.0115(10)	1.2
$HC^{13}CCCCN$	18–17	47436.1316(28)	0.013	5.86(30)	0.56(07)	0.0078(10)	1.5
$HCC^{13}CCCN$	12–11	31918.6866(18)	0.038	5.87(08)	0.65(02)	0.0258(10)	0.7
$HCC^{13}CCCN$	13–12	34578.5381(19)	0.033	5.86(05)	0.72(01)	0.0256(10)	0.6
$HCC^{13}CCCN$	14–13	37238.3802(21)	0.033	5.86(07)	0.65(02)	0.0227(10)	0.6
$HCC^{13}CCCN$	15–14	39898.2122(22)	0.031	5.88(06)	0.60(01)	0.0199(10)	0.7
$HCC^{13}CCCN$	16–15	42558.0335(23)	0.028	5.87(09)	0.53(02)	0.0156(10)	0.8
$HCC^{13}CCCN$	17–16	45217.8432(24)	0.025	5.89(15)	0.65(04)	0.0169(10)	1.3
$HCC^{13}CCCN$	18–17	47877.6406(26)	0.015	5.86(30)	0.49(07)	0.0079(10)	1.7
$HCCC^{13}CCN$	12–11	31922.5700(16)	0.036	5.82(08)	0.68(02)	0.0264(10)	0.7
$HCCC^{13}CCN$	13–12	34582.7452(17)	0.032	5.81(07)	0.69(02)	0.0232(10)	0.6
$HCCC^{13}CCN$	14–13	37242.9110(18)	0.033	5.83(08)	0.67(02)	0.0234(10)	0.8
$HCCC^{13}CCN$	15–14	39903.0667(19)	0.030	5.84(06)	0.58(01)	0.0183(10)	0.7
$HCCC^{13}CCN$	16–15	42563.2117(20)	0.027	5.84(08)	0.56(02)	0.0163(10)	0.9
$HCCC^{13}CCN$	17–16	45223.3451(21)	0.023	5.81(12)	0.53(03)	0.0128(10)	1.1
$HCCC^{13}CCN$	18–17	47883.4663(22)	0.021	5.86(27)	0.61(06)	0.0135(10)	1.7

Notes. [a]Except when indicated, it corresponds to the group of the three strongest hyperfine components ($\Delta F = 1$). [b]Adopted rest frequencies (see text). [c]Local standard of rest velocity of the emission for the adopted rest frequency (in kms^{-1}). [d]Linewidth at half intensity derived by fitting a Gaussian line profile to the observed transitions (in kms^{-1}). [e]Integrated line intensity in K kms^{-1}. [f]The sensitivity of the data (root mean square error) has been derived from a baseline to the each line in a velocity window −6.2 to 17.8 km s^{-1} (in mK). [g]Line fully blended with a strong negative feature produced by the frequency switching observing procedure.

Table B.3. continued.

Molecule	J_u–J_l [(a)]	$\nu_{\rm rest}$ [(b)] (MHz)	T_A^* (K)	$v_{\rm LSR}$ [(d)] (kms^{-1})	Δv [(e)] (kms^{-1})	$\int T_A^* {\rm d}v$ [(c)] (K kms^{-1})	σ [(f)] (mK)
HCCCC^{13}CN	12–11	31636.1315(14)	0.042	5.86(07)	0.66(02)	0.0294(10)	0.8
HCCCC^{13}CN	13–12	34272.4373(15)	0.036	5.81(05)	0.72(01)	0.0277(10)	0.5
HCCCC^{13}CN	14–13	36908.7338(16)	0.038	5.84(05)	0.66(01)	0.0263(10)	0.6
HCCCC^{13}CN	15–14	39545.0204(17)	0.033	5.85(05)	0.61(01)	0.0216(10)	0.7
HCCCC^{13}CN	16–15	42181.2963(18)	0.034	5.85(06)	0.54(02)	0.0193(10)	0.8
HCCCC^{13}CN	17–16	44817.5608(19)	0.025	5.84(11)	0.60(03)	0.0156(10)	1.0
HCCCC^{13}CN	18–17	47453.8132(20)	0.020	5.86(16)	0.63(04)	0.0132(10)	1.3
HCCCCC^{15}N	12–11	31167.1619(15)	0.010	5.90(35)	0.61(06)	0.0064(10)	0.9
HCCCCC^{15}N	13–12	33764.3882(17)	0.007	5.80(24)	0.64(07)	0.0045(10)	0.5
HCCCCC^{15}N	14–13	36361.6056(18)	0.010	5.75(21)	0.81(05)	0.0084(10)	0.6
HCCCCC^{15}N	15–14	38958.8134(19)	0.010	5.75(22)	0.83(05)	0.0087(10)	0.6
HCCCCC^{15}N	16–15	41556.0109(20)	0.007	5.81(33)	0.57(07)	0.0042(10)	0.8
HCCCCC^{15}N	17–16	44153.1975(21)	0.007	5.84(44)	0.53(10)	0.0039(10)	1.2
HCCCCC^{15}N	18–17	46750.3723(22)	0.007	5.79(27)	0.54(08)	0.0039(10)	1.2
DC_5N	13–12	33047.2676(05)	0.040	5.84(01)	0.66(02)	0.0284(10)	0.6
DC_5N	14–13	35589.3244(05)	0.037	5.86(01)	0.66(01)	0.0260(10)	0.6
DC_5N	15–14	38131.3723(05)	0.036	5.86(01)	0.62(02)	0.0238(10)	0.5
DC_5N	16–15	40673.4104(06)	0.038	5.87(01)	0.51(01)	0.0205(10)	0.7
DC_5N	17–16	43215.4382(06)	0.029	5.89(01)	0.49(02)	0.0151(10)	1.0
DC_5N	18–17	45757.4551(07)	0.022	5.88(02)	0.70(05)	0.0167(10)	1.3
DC_5N	19–18	48299.4603(07)	0.016	5.79(04)	0.56(07)	0.0097(10)	1.7
HC_7N	28–27	31583.7088(10)	0.320	5.85(02)	0.63(01)	0.2147(10)	0.8
HC_7N	29–28	32711.6717(10)	0.272	5.84(02)	0.67(01)	0.1946(10)	0.6
HC_7N	30–29	33839.6318(10)	0.229	5.83(02)	0.71(01)	0.1722(10)	0.5
HC_7N	31–30	34967.5890(10)	0.203	5.85(02)	0.69(01)	0.1480(10)	0.5
HC_7N	32–31	36095.5431(11)	0.189	5.86(02)	0.64(01)	0.1298(10)	0.7
HC_7N	33–32	37223.4942(11)	0.168	5.85(02)	0.63(01)	0.1134(10)	0.6
HC_7N	34–33	38351.4420(12)	0.147	5.86(02)	0.60(02)	0.0938(10)	0.7
HC_7N	35–34	39479.3866(12)	0.124	5.87(02)	0.58(02)	0.0766(10)	0.6
HC_7N	36–35	40607.3277(12)	0.113	5.87(02)	0.52(02)	0.0624(10)	0.9
HC_7N	37–36	41735.2654(12)	0.092	5.87(03)	0.49(02)	0.0476(10)	1.1
HC_7N	38–37	42863.1995(13)	0.077	5.87(03)	0.51(03)	0.0415(10)	0.9
HC_7N	39-38 [(g)]	43991.1299(13)					1.0
HC_7N	40–39	45119.0565(13)	0.047	5.87(02)	0.54(03)	0.0270(10)	1.4
HC_7N	41–40	46246.9792(13)	0.043	5.87(02)	0.46(03)	0.0210(10)	1.3
HC_7N	42–41	47374.8980(14)	0.022	5.88(03)	0.49(04)	0.0116(10)	1.5
HC_7N	43–42	48502.8127(14)	0.018	5.78(02)	0.64(06)	0.0125(10)	1.7
HC_7N	44–43	49630.7232(14)	0.013	5.95(06)	0.57(12)	0.0076(10)	2.1

Appendix C: Quantum chemical calculations for the HC_5N isomers

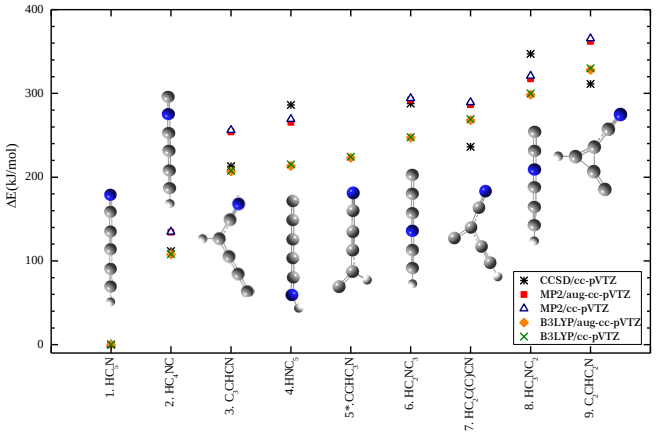

Fig. C.1. Theoretical energies found at different levels of theory for the HC_5N isomers that stand below 500 kJ mol^{-1}. The isomers are represented from the optimized coordinates obtained at MP2/cc-pVTZ level of theory, except for those marked with an asterisk in their name, where the B3LYP/aug-cc-pVTZ structures were used, see text of Appendix C.

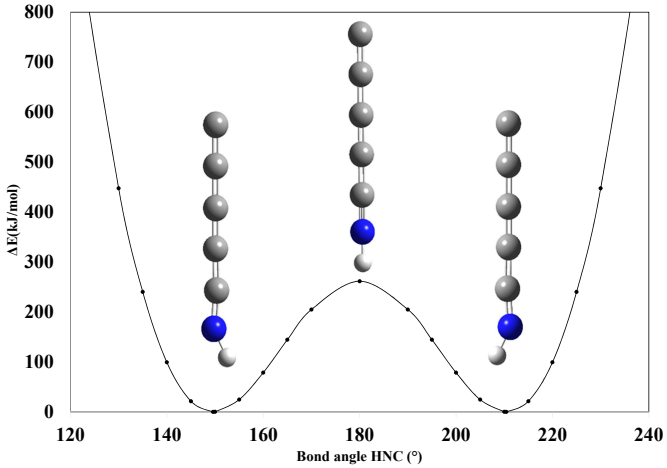

Fig. C.2. Potential energy well obtained by evaluating the HNC bond angle of the HNC_5 species (**4**).

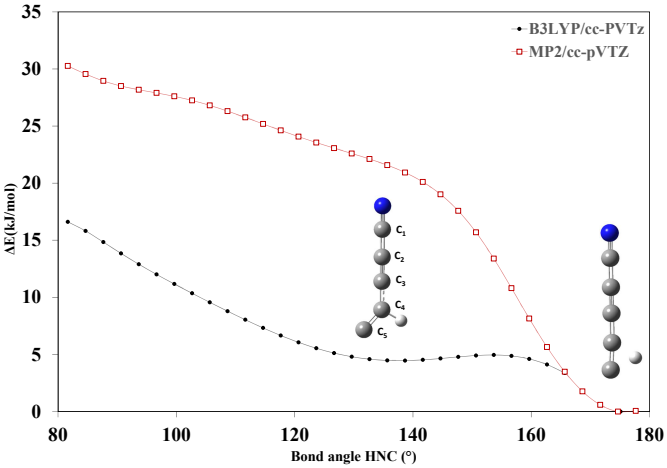

Fig. C.3. Potential energy scan of the C_3 C_4 C_5 bond angle for the **5** species ($CCHC_3N$) evaluated at MP2/cc-pVTZ and B3LYP/cc-pVTZ levels of theory.

The relative stability between the possible isomers of HC_5N has been evaluated by different quantum chemical calculations. As initial values for our calculations, we took the optimized structures present in the literature (Gronowski & Kołos 2006, 2007). We optimized these structures using sequential calculation methods in oder of complexity: first, the density functional theory (DFT) hybrid exchange-correlation variant (B3LYP), then the Møller-Plesset second-order perturbation theory (Møller & Plesset 1936), and, finally, closed-shell coupled cluster with singles and doubles (CCSD) (Cížek 1969). For all these methods, we used the Dunning's correlation consistent polarized valence triple-ζ basis sets (cc-pVTZ), and, in the case of the DFT and MP2 methods, we increased the basis sets with diffuse functions (aug-cc-pVTZ), see Fig. C.1. Besides the optimization, we have calculated some relevant parameters such as the vibrational energies, IR intensities and the rotational constants at the vibrational ground state, thanks to the frequency calculations using the MP2/cc-pVTZ level of theory under anharmonic corrections (see Table C.1). All these calculations were performed using the Gaussian 09 (Frisch et al. 2013) software package.

The energy order of the HC_5N isomers does not drastically change as a function of the level of theory assumed. As expected, the two most stable isomers are HC_5N (**1**) and HC_4NC (**2**), separated in energy by ~110 kJ mol^{-1}. In the 200−400 kJ mol^{-1} range, we found seven different species, including: additional linear structures (or quasi linear) such as: HNC_5 (**4**), HC_2NC_3 (**6**), and HC_3NC_2 (**8**); a cyclic species (C_2CHC_2N (**9**); and branched structures: C_3CHCN (**3**), $CCHC_3N$ (**5**)), $HC_2C(C)CN$ (**6**). In case of the quasi linear structure HNC_5 (**4**), we verified the non-linearity of its structure by calculating the potential well; see Fig. C.2. As pointed out in the literature (Gronowski & Kołos 2006), some branched isomers are more stable that the linear structures. Nevertheless, we found some difficulties in finding the minimum energy potential for some of these branched species: **5** and **7**.

Species **5**, $CCHC_3N$, was considered the one with lowest energy among the branched C_5HN isomers in the literature (Gronowski & Kołos 2006, 2007). The relative stability of $CCHC_3N$ compared to other linear structures has led a number of authors to propose it, together with the two carbon less analogue, CCHCN, as good candidates for searches in space. In our calculations, we could find the optimized structure **5** using the B3LYP method, however, neither the MP2 or CCSD converged to this structure. To understand the non-convergence to this structure, we analyzed the potential energy along the C_3 C_4 C_5 bond angle and we compared the results between the B3LYP and MP2 methods; see Fig. C.3. For the structure in the B3LYP calculation, we found a minimum at a C_3 C_4 C_5 bond angle of 137°. In contrast, for the MP2 calculations, any potential well was found around this angle. The only stable structure obtained with MP2 and CCSD methods corresponds to a species where the hydrogen is no longer covalently linked to the carbon chain which is linearly bounded.

Another isomer that should be pointed out is the species **7**,$HC_2C(C)CN$ since the bond angle around the branching structure C_4 C_2 C_3 has a non-conventional value of ~90°. A similar structure was proposed between the most stables isomers by Gronowski & Kołos (2006). However, calculations by the same author in 2007 indicated that the bond angle of the optimized

Table C.1. Energies, rotational constants, quadrupole coupling constants, dipole moment, and vibrational partition functions of the HC_5N isomers evaluated at MP2/cc-pVTZ level of theory.

	ΔE [a] (kJ mol^{-1})	ΔE_{MP2} [b] (kJ mol^{-1})	A_0 [c] (MHz)	B_0 [c] (MHz)	C_0 [c] (MHz)	$1.5\chi_{aa}$ (MHz)	$0.25(\chi_{bb}-\chi_{cc})$ (MHz)	μ_T (D)	Q_v [d] 50 K	Q_v [d] 300 K
HC_5N [e]	0.0	0.0		1320.046		−5.77		4.36	1.09	22.89
HC_4NC [f]	134.7	133.8		1390.737		1.15		3.57	1.07	22.62
C_3CHCN	256.1	254.5	21076.776	1689.938	1564.496	−2.73	−0.41	3.09	1.10	14.18
C_5NH	269.2	267.7		1348.267		2.10	0.31	9.14	1.02	8.86
HC_2NC_3	294.1	292.2		1434.147		2.96		6.58	1.01	8.06
$HC_2C(C)CN$	289.3	284.2	10693.657	2526.651	2038.799	−4.72	−0.20	3.27	1.06	15.93
HC_3NC_2	320.8	316.2		1435.856		0.91		7.15	1.03	15.46
C_2CHC_2N	365.5	361.3	11195.360	2552.013	2073.245	−5.24	−0.14	4.48	1.15	15.16

Notes. [a]Relative energy to the lowest energy isomer HC_5N evaluated at MP2/cc-pVTZ level of theory. [b]Relative energy including the zero-point correction energy calculated for each species. [c]Rotational constants at the ground state evaluated using the vibration-rotation interaction constants obtained using the anharmonic corrections. In the case of the quasi linear C_5NH, the effective rotational constant, B_{eff}, is provided. [d]Vibrational partition function calculated using the expression $\prod_i(1-e^{-(h\omega_i/KT)})^{-d_i}$ (Gordy & Cook 1984), where ω_i and d_i represent the energy and the degeneracy of each i vibrational mode. The energies for the vibrational modes are taken from the results of ab initio calculations evaluated at MP2/cc-pVTZ level of theory, under the anharmonic correction. At the temperature of TMC1 (10 K), the vibrational partition function for isomers is equal to one. [e]The experimental value is $B_0 = 1331.33269 \pm 0.00002$ (Bizzocchi et al. 2004). The ratio $B_0(\text{exp})/B_0(\text{Cal})$ is 1.0086. [f]The experimental value is $B_0 = 1401.18216 \pm 0.00006$ (this work, see Table A.3. The ratio $B_0(\text{exp})/B_0(\text{Cal})$ is 1.0075.

structure was ∼120° (Gronowski & Kołos 2007). Our scan along the C_4 C_2 C_3 bond angle (Fig. C.4) at MP2/cc-pVTZ level of theory does not show any potential minima at the ∼120° angle. The only structures that converged in the calculations are those corresponding to zero degrees, that is, the species **1**, and the ∼90° one. Neither the cyclic structure or the ∼120° converged with the MP2 methodology. In contrast, CCSD calculations show that the real minima is at ∼120° bond angle, which is the reason why the energy at CCSD is lower than the one at MP2 calculations.

Independently of the level of theory employed in the calculations, the two observed species in space, HC_5N (**1**) and HC_4NC (**2**), are the most stable isomers of cyanodiacetylene.

The rotational constants we have calculated for the different isomers of HC_5N are precise enough to search for them in space. However, we could expect very weak lines, which would be well below those of HC_4NC. Hence, the possibility to detect them in interstellar clouds without precise laboratory frequencies is rather unlikely.

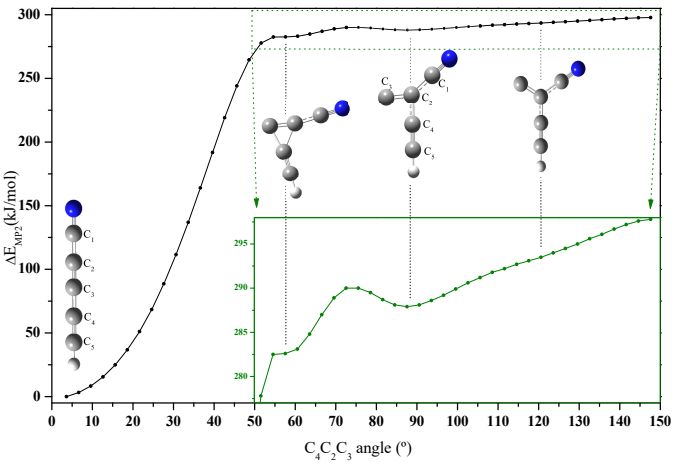

Fig. C.4. Potential energy scan of the C_4 C_2 C_3 bond angle for the isomer $HC_2C(C)CN$ (**6**) evaluated at MP2/cc-pVTZ.